International Journal of Minerals, Metallurgy and Materials
Volume 22, Number 7, July 2015, Page 762
DOI: 10.1007/s12613-015-1132-9

Large-scale synthesis of nickel sulfide micro/nanorods via a hydrothermal process

Peng-fei Yin[1)], *Xiang-yu Han*[1)], *Chao Zhou*[2)], *Chuan-hui Xia*[1)], *Chun-lian Hu*[1)], *and Li-li Sun*[3)]

1) College of Science, Chongqing Jiaotong University, Chongqing 400074, China
2) Department of Materials Science, Chongqing Jiaotong University, Chongqing 400074, China
3) Department of Physics, Third Military Medical University, Chongqing 400038, China
(Received: 12 October 2014; revised: 12 March 2015; accepted: 17 March 2015)

Abstract: Rhombohedral-phase NiS micro/nanorods were synthesized on a large scale through a hydrothermal method using $NiCl_2·6H_2O$ and thiourea crystals as starting precursors. Recrystallized thiourea was observed to play an important role in the formation of micro/nanosized rods and flower-like structures. The molar ratio and reaction temperature of the precursors influenced the morphology and phase of NiS products. Pure rhombohedral NiS micro/nanorods were obtained on a large scale when the molar ratio between $NiCl_2·6H_2O$ and thiourea crystals was fixed at 2:1, and the mixture was heated at 250°C for 5 h. Flower-like NiS nanostructures were formed when the molar ratio between $NiCl_2·6H_2O$ and thiourea crystals was maintained at 1:1. The Raman and Fourier-transform infrared (FTIR) spectra of the as-prepared rhombohedral NiS micro/nanorods were collected, and their magnetic properties were investigated. The results showed that the FTIR absorption peaks of the as-prepared product are located at 634 cm^{-1} and their Raman peaks are located at 216 and 289 cm^{-1}; the as-prepared NiS micro/nanorods exhibited weak ferromagnetic behavior due to the size effect.

Keywords: nickel sulfide; nanorods; hydrothermal synthesis; optical properties; magnetic measurement

1. Introduction

As a semiconductor-related material, nickel sulfide, which is a typical 3d transition metal sulfide, can form various phases such as NiS, $Ni_{3+x}S_2$, Ni_3S_2, Ni_7S_6, Ni_9S_8, Ni_3S_4, and NiS_2. Among these phases, NiS has attracted increasing attention recently for its attractive electrochemical [1–2], high-performance supercapacitor [3], optical [4], electrocatalytic [5], and magnetic properties [6], which promote its application in various fields. Among other applications, it has been used as a cathode material in rechargeable lithium or secondary batteries [7–11], as a supercapacitor [3] in dye-sensitized solar cells [5,12–13], as a photocatalyst [14–15], and as an improved Na- and Li-storage material [16–17]. As is known, the properties of materials are highly dependent on their structures. Thus far, various morphologies of rhombohedral NiS have been synthesized, including chain-like tubes [18] and layer-rolled [19], urchin-like [20–21], flower-like [22–24], and hierarchical carnation-like [25] nanorods [26] and triangular nanoprisms [27]. Numerous methods have been employed to synthesize rhombohedral NiS, including solvothermal synthesis [28], cyclic microwave radiation synthesis [29], and solid–solid reactions [30]. In particular, the solvothermal method has been demonstrated to be an effective synthetic technique for preparing high-purity, well-dispersed chalcogenides with controllable phases and morphologies [31–33].

One-dimensional materials, such as nanowires, nanorods, and nanotubes, have stimulated great interest because of both of the unique electrical and optical properties associated with their dimensionality and their wide range of potential applications in nanodevices. In this study, nickel sulfide micro/nanostructures were synthesized under various S/Ni molar ratios and reaction times through a solvothermal method in which $NiCl_2·6H_2O$ and thiourea crystals were used as reactants. The properties of the as-prepared NiS micro/nanorods were investigated using Raman spectroscopy, Fourier-transform infrared (FTIR) spectroscopy, and mag-

Corresponding author: Li-li Sun E-mail: suntmmu@163.com

netic property measurements.

2. Experimental

All the analytical chemicals were used without further purification. In a typical procedure, 0.005 mol of thiourea powder was added to 10 mL of distilled water with intensive stirring to form a clear, colorless solution that was subsequently allowed to evaporate in a drying oven at 50°C to obtain good quality thiourea crystals. 10 mmol of $NiCl_2{\cdot}6H_2O$ was subsequently added to 20 mL of distilled water with intensive stirring to form a dark-green solution; the sulfur source, thiourea crystals, was then added to this solution. The obtained mixtures were then transferred to a Teflon-lined stainless steel autoclave with a capacity of 30 mL. The mixtures were heated in the autoclave at 250°C for 5 h and then allowed to cool to room temperature naturally. After the autoclave contents were filtered, washed with distilled water and ethanol several times, and dried in air at 80°C for 5 h, the final products were obtained. To better understand the morphological evolution of the synthesized products, we combined the precursors in different molar ratios and heated the mixtures for different periods of time.

The X-ray powder diffraction (XRD) patterns of products were recorded on a XD-2 X-ray diffractometer equipped with a Cu K_α radiation source (λ = 0.154187 nm); samples were scanned over the 2θ range from 20° to 70° at a scanning speed of 2°/min. Scanning electron microscope (SEM) images were collected with a KYKY2800B scanning electron microscope. Transmission electron microscope (TEM) images were obtained on a Tecnai G2 20 TEM operated at an accelerating voltage of 200 kV. The FTIR spectra were recorded with a Perkin–Elmer Spectrum One FTIR spectrometer using the KBr pellet technique; the samples were scanned in the range from 400 to 4000 cm^{-1}. Raman spectra were recorded with a Renishaw InVia laser Raman spectrometer. The magnetic measurements were conducted at room temperature in a vibrating sample magnetometer (MPMS-XL-7).

3. Results and discussion

The synthesized NiS micro/nanocrystals were characterized by powder XRD to confirm their crystal structure and chemical composition. Fig. 1 shows a typical XRD pattern of the product prepared at 250°C for 5 h using $NiCl_2{\cdot}6H_2O$ and recrystallized thiourea crystals as reactants in a molar ratio of 2:1. All peaks were clearly indexed as rhombohedral NiS, which is consistent with the literature data (JCPDS card No. 12-0041, space group *R*3*m*). No impurities were detected in this pattern, which indicates that pure NiS can be obtained under the current synthetic conditions. The sharp peaks in the XRD pattern indicate that good quality crystals were obtained and that the crystals grew primarily along with the (300) direction. The average crystallite size of the products synthesized at 250°C was calculated using Scherrer's equation:

$$D = \frac{0.89\lambda}{\beta \cos\theta},$$

where D is the average crystallite dimension, λ is the wavelength of incident X-rays, θ is the diffraction angle, and β is the full width at half maximum. The calculated average crystallite size was 54.5 nm for NiS products prepared at 250°C for 5 h using $NiCl_2{\cdot}6H_2O$ and thiourea crystals in a molar ratio of 2:1.

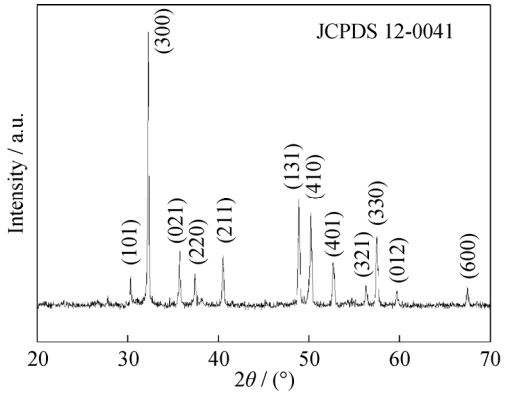

Fig. 1. XRD pattern of NiS micro/nanorods prepared at 250°C for 5 h in water using $NiCl_2{\cdot}6H_2O$ and thiourea at a molar ratio of 2:1.

The sizes and morphologies of the as-prepared products were characterized by SEM and TEM. Fig. 2(a) shows a low-magnification SEM image of the as-prepared rhombohedral NiS micro/nanorods obtained at 250°C for 5 h using $NiCl_2{\cdot}6H_2O$ and thiourea crystals in a molar ratio of 2:1; this image indicates that the products were composed of a large number of micro/nanorods and were obtained in high yield. Fig. 2(b) is a representative high-magnification SEM image of the as-prepared rhombohedral NiS micro/nanorod crystals. As evident in Fig. 2(b), the as-prepared rhombohedral NiS products were composed of nanosized and microsized rods. The microsized NiS crystals were approximately 1 μm in width and 10 μm in length, and the nanosized rods were estimated to be approximately 100 nm in width. TEM was used to obtain an overall view of the nanosized rods. Fig. 2(c) shows a TEM image of the as-prepared rhombohedral NiS nanorods. The width of the nanosized rhombohedral NiS rods was approximately 50 nm, which is similar to the average crystallite size calculated using Scherrer's equation.

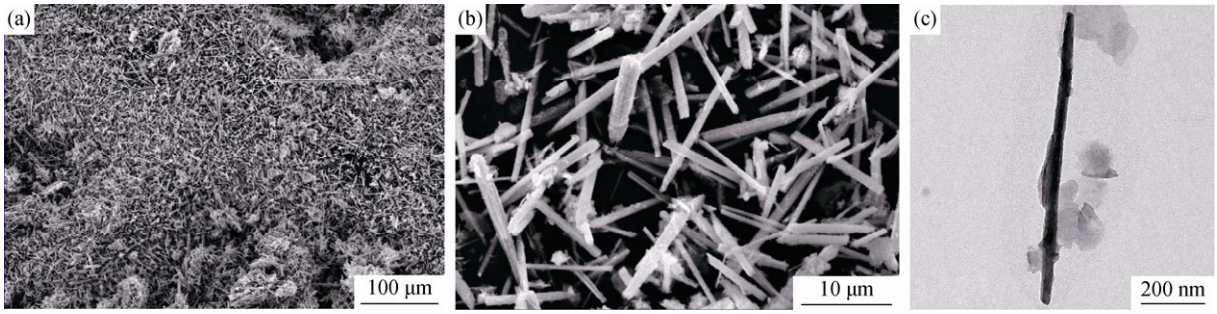

Fig. 2. SEM images (a,b) and TEM image (c) of as-prepared NiS micro/nanorods synthesized at 250°C for 5 h with $NiCl_2·6H_2O$ and recrystallized thiourea at a molar ratio of 2:1.

Normally, irregular particles are formed in homogeneous aqueous solutions of $NiCl_2·6H_2O$ and thiourea [34]. Figs. 3(a) and 3(b) show the SEM images of the as-prepared products obtained from an $NiCl_2·6H_2O$ and thiourea homogenous solution with a Ni^{2+}/thiourea molar ratio of 1:1 at 250°C for 5 h; irregular particles were obtained. However, when the recrystallized thiourea was added to $NiCl_2$ solution and the recrystallized Ni^{2+}/thiourea molar ratio was fixed at 1:1, the morphology of the product changed substantially; micrometer-sized, flower-like architectures with few irregular particles were formed (Figs. 3(c) and 3(d)). We observed that the flower-like architectures were composed mainly of

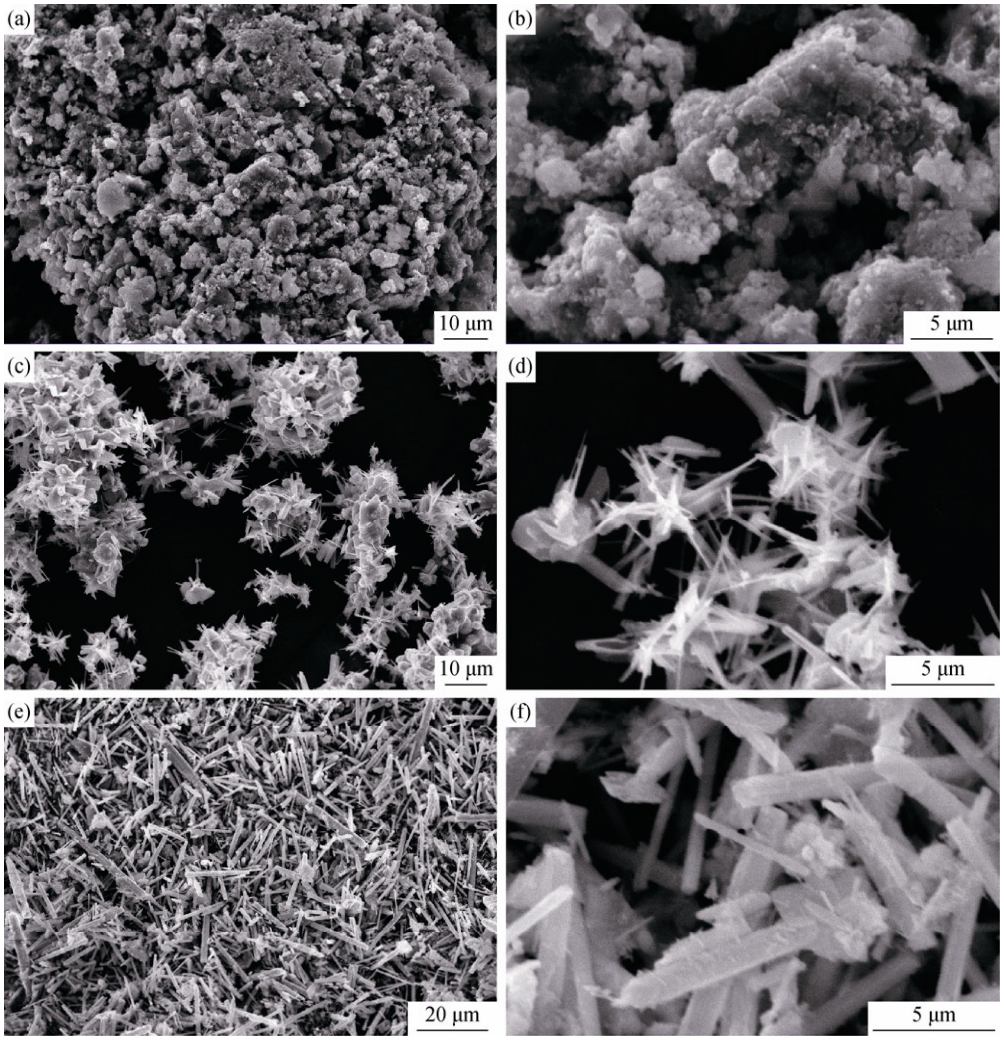

Fig. 3. (a,b) SEM images of the as-prepared products synthesized at 250°C for 5 h using a $NiCl_2·6H_2O$ and thiourea homogenous solution at a molar ratio of 1:1; SEM images of the as-prepared products obtained from the reaction of $NiCl_2·6H_2O$ and recrystallized thiourea at molar ratios of 1:1 (c,d) and 2:1 (e,f) at 250°C for 5 h.

nanosized rods with diameters of approximately 100 nm and lengths up to 5 μm. When the recrystallized Ni^{2+}/thiourea molar ratio was maintained at 2:1, large-scale micro/nanorods were observed instead of flower-like architectures, as shown in Figs. 3(e) and 3(f). As evident in the images, the diameter and length of the microsized rods were approximately 1 μm and 10 μm, respectively, and the diameter and length of the nanosized rods were approximately 100 nm and 1 μm, respectively. Interestingly, the nanosized and microsized rods have similar length–diameter aspect ratios. The recrystallization of thiourea and the molar ratios of the precursor obviously influenced the morphologies of the final product. As previously mentioned, the process of recrystallization of thiourea is speculated to be very important in the formation of oriented structures. Thiourea powders are easily dissolved by water; however, the process of recrystallization changes the thiourea powders to a bulk crystalline material, which makes complete dissolution of thiourea in solution difficult when the reaction occurs. The rest of undissolved crystalline thiourea might enhance the anisotropy of solution and play an assisting role in the formation of the micro/nanorods.

Thiourea is commonly used as a precursor in the synthesis of NiS nanostructures, and an excess of thiourea is always added to the reaction mixtures to achieve a sulfur-rich condition; however, the excess of thiourea may lead to the unnecessary release of toxic gas. Obviously, the risk of poisonous waste gas release in the experiment is diminished when large-scale micro/nanorods are prepared because the molar ratio of $NiCl_2{\cdot}6H_2O$ and thiourea is more than 1. The reaction process can be speculated as follows:

$$NiCl_2 + SC(NH_2)_2 + 2H_2O \xrightarrow{250°C}$$

$$2NH_3 + CO_2 + 2HCl + NiS\,.$$

Micro/nanorods were prepared in deionized water as a solvent without using any organic solution, which makes the waste reaction liquid easy to handle.

Figs. 4(a)–4(e) display the SEM images of the products prepared at 250°C with a molar ratio of $NiCl_2{\cdot}6H_2O$ and thiourea crystals of 1:1 for different reaction time periods. The images clearly reveal the morphological evolution of the as-prepared products with increasing reaction time. As shown in Fig. 4(a), when the reaction time was maintained at 1 h, the products were mainly composed of irregular particles with little flower-like architecture. When the reaction time was extended to 2 h, the density of irregular particles decreased and the number of flower-like architectures increased (Fig. 4(b)). When the reaction time was extended to 5 h, we observed that the as-prepared products consisted primarily of flower-like architectures, although a few irregular particles remained (Fig. 4(c)). Fig. 4(d) shows an enlarged image of Fig. 4(c), indicating that the flower-like structures are composed of nanorods with a diameter of approximately 200 nm and lengths as long as 5 μm. When the reaction time was increased to 10 h, the flower-like structures which were composed of nanosized and microsized rods were obtained, as shown in Fig. 4(e). The diameter and length of the microsized rods were approximately 1 μm and 5 μm, respectively, and the diameter and length of the nanosized rods were approximately 100 nm and 2 μm, respectively. These results demonstrate that the reaction time can affect the morphology of the as-prepared products. The thiourea being crystalline may enhance the anisotropy of the solution, which, in turn, can facilitate the formation of nuclei at the beginning of the reaction. With a continuous supply of the building blocks, these nuclei can serve as seeds for further growth to form larger structures; flower-like structures are produced with increasing reaction time, and the rods, which consist of flower-like architectures, become thicker and longer, and then a part of the nanosized rods which consist of the flower-like structures grow to microsized rods. Therefore, the flower-like structures composed of nanosized and microsized rods are formed. Given the highly complex phase diagram of NiS, in most of cases, obtaining pure phases of NiS is difficult; a mixture of two or more phases is typically obtained [27,35–37]. Fig. 4(f) shows the XRD pattern of NiS prepared at 250°C for 10 h using a $NiCl_2{\cdot}6H_2O$/thiourea molar ratio of 1:1; the diffraction peaks can be indexed as a mixture of cubic Ni_3S_4 (JCPDS 47-1739) and low-temperature-phase rhombohedral NiS (JCPDS 12-0041). The average crystallite size of cubic Ni_3S_4 and low-temperature-phase rhombohedral NiS were also calculated using Scherrer's equation. The results show that the average crystallite size of rhombohedral NiS was 53.8 nm and larger than that of cubic Ni_3S_4 (30.5 nm).

For further confirmation and characterization, the Raman spectrum of the as-prepared rhombohedral NiS was collected at room temperature. Fig. 5(a) displays the room-temperature Raman spectrum of the as-prepared rhombohedral NiS micro/nanorods. Theoretically, there are eight Raman-active vibrational frequencies at the Γ point of millerite NiS; these vibrations can be classified as $\Gamma_{\text{Raman}}(\text{NiS}) = 3A_1 + 5E$ [38]. With respect to the as-prepared rhombohedral NiS micro/nanorods, the Raman spectrum exhibits two peaks that originate from two different active modes. The vibrational frequency peaks located at 216 and 289 cm^{-1} partly agree well with previously reported results [39]. As

shown in Fig. 5(a), the peaks located at 216 and 289 cm^{-1} should correspond to the A_1 mode and E mode, respectively. The locations of these peaks slightly differ from the theoretical locations reported by Wang *et al.* [38].

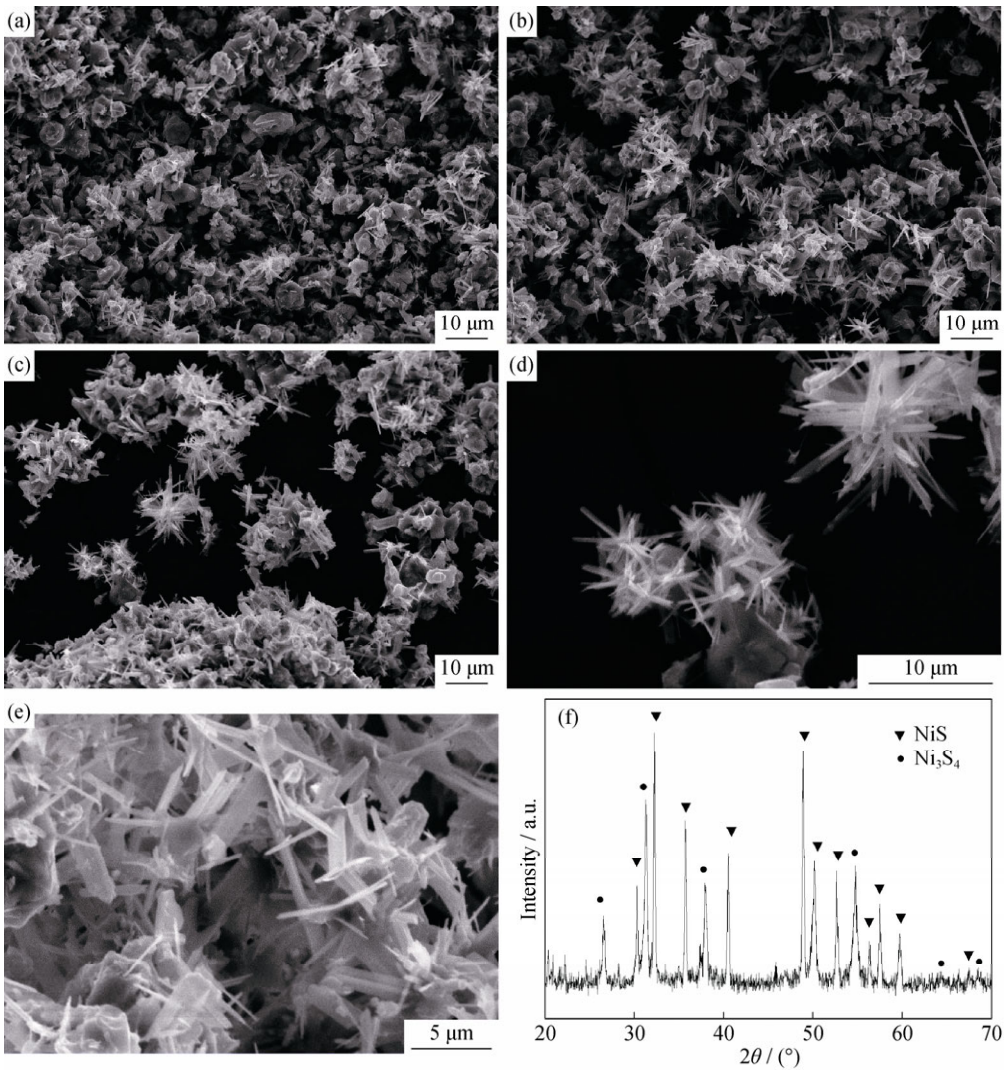

Fig. 4. (a–e) SEM images of the as-prepared products obtained from the reaction of $NiCl_2·6H_2O$ and thiourea crystals at a molar ratio of 1:1 at 250°C for different reaction time periods: (a) 1 h, (b) 2 h, (c,d) 5 h, and (e) 10 h; (f) XRD pattern of NiS prepared at 250°C for 10 h using $NiCl_2·6H_2O$ and thiourea at a molar ratio of 1:1.

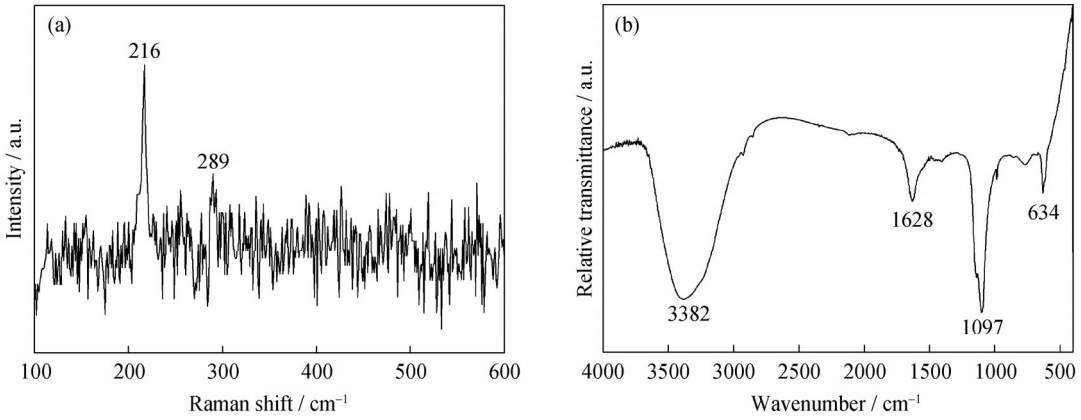

Fig. 5. Room-temperature Raman spectrum (a) and FTIR spectrum (b) of NiS micro/nanorods prepared at 250°C for 5 h.

We used FTIR to study the infrared absorption properties of the as-prepared NiS micro/nanorods. Fig. 5(b) shows the 400–4000 cm^{-1} range of the FTIR spectrum of the as-prepared rhombohedral NiS micro/nanorods synthesized at 250°C for 5 h. The FTIR spectrum of the product shows absorption peaks at 3382, 1628, 1097, and 636 cm^{-1}. The absorption peaks at 3382 and 1628 cm^{-1} can be assigned to the stretching and bending vibrations, respectively, of the OH groups of H_2O. The peak observed at 1097 cm^{-1} is assigned to the C–O stretching vibration originating from the adsorption of CO_2, which may originate from the atmosphere or from the reaction. The bands at 634 cm^{-1} are attributable to the Ni–S stretching vibration modes in NiS.

The magnetic properties of nanomaterials are highly dependent on the structure, morphology, and geometry of the material. To investigate the magnetic properties of the as-prepared NiS micro/nanorods architectures, remanent magnetization (M_r) and coercive force (H_c) data were acquired. Fig. 6 displays the curve of magnetization vs. applied magnetic field (M–H) collected at room temperature for the as-synthesized NiS micro/nanorod architectures; the results show that the M_r and H_c are 0.00047 emu/g and 16.79 Oe, respectively. These results indicate that the as-obtained material exhibits some weak ferromagnetic interactions, even though bulk NiS is antiferromagnetic [40–41]. In 1961, Néel suggested that fine particles of an antiferromagnetic material should exhibit magnetic properties such as superparamagnetism and weak ferromagnetism [42]. In recent years, anomalous magnetic properties have been observed for NiS nanostructures. For example, Zhang *et al.* [40] reported that NiS exhibits a remanent magnetization of 0.00012 emu/g and a coercivity of 155 Oe, whereas Salavati-Niasari *et al.* [43] reported an M_r and H_c of 0.0011 emu/g and 154 Oe, respectively, and Cao *et al.* [44] reported an M_r and H_c of 0.006 emu/g and 178 Oe, respectively, for the same material. These weak ferromagnetic behaviors might arise from the so-called finite-size effect and/or from modification of the bulk state due to surface effects [45]. This explanation suggests that the long-range antiferromagnetic order is destroyed in nanoscale materials [46]. The as-prepared NiS micro/nanorods also display similar magnetic behavior that could be due to the surface effect; however, the obtained NiS product exhibits a much lower remanent magnetization (M_r) and coercive force (H_c) than those reported by Cao *et al.* [44], which may contribute to the particle size of the as-prepared product. The product is composed mainly of nanorods with a diameter of approximately 50 nm and microrods with a diameter of 1–2 μm. The microsized structures may display magnetic behavior similar to that of the bulk; however, the nanosized rods existing in the product may be the reason for displaying weak ferromagnetic behavior due to the size effect.

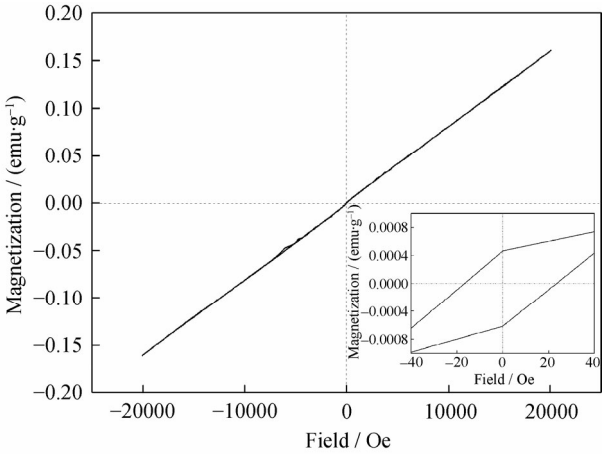

Fig. 6. Room temperature magnetic hysteresis loop of NiS micro/nanorods synthesized at 250°C for 5 h.

4. Conclusion

In summary, large-scale rhombohedral NiS micro/nanorods have been prepared through a hydrothermal method at 250°C using $NiCl_2 \cdot 6H_2O$ and thiourea crystals as reactants. Recrystallized thiourea was observed to play an important role in the formation of micro/nanosized rods and flower-like structures, and the molar ratio and reaction temperature were observed to influence the morphology and phase of NiS products. Large-scale pure rhombohedral NiS micro/nanorods were obtained when the S/Ni molar ratio was fixed at 1:2. The properties of the as-prepared, pure rhombohedral NiS micro/nanorods were investigated. FTIR results showed that rhombohedral NiS micro/nanorods absorb at 634 cm^{-1}, and their Raman spectrum exhibited peaks at 216 and 289 cm^{-1}; the magnetic properties of the as-prepared NiS micro/nanorods exhibited weak ferromagnetic behavior because of the size effect.

Acknowledgements

This study was financially supported by the National Science Foundation of China (Nos. 11305274 and 11304407) and by the Natural Science Foundation of Chongqing City, China (No. cstc.2011jja50005).

References

[1] H.S. Ryu, C.W. Ha, S.Y. Ji, I.S. Ahn, J.H. Ahn, H.J. Ahn,

and K.W. Kim, Electrochemical properties of the NiS powder prepared by co-precipitation method for lithium secondary battery, *J. Nanosci. Nanotechnol*., 14(2014), No. 10, p. 7943.

[2] J.Q. Yang, X.C. Duan, W. Guo, D. Li, H.L. Zhang, and W.J. Zheng, Electrochemical performances investigation of NiS/rGO composite as electrode material for supercapacitors, *Nano Energy,* 5(2014), p. 74.

[3] X.Y. Yan, X.L. Tong, L. Ma, Y.M. Tian, Y.S. Cai, C.W. Gong, M.G. Zhang, and L.P. Liang, Synthesis of porous NiS nanoflake arrays by ion exchange reaction from NiO and their high performance supercapacitor properties, *Mater. Lett.,* 124(2014), p. 133.

[4] S.C. Yan, Y. Shi, L.T. Sun, Z.D. Xiao, B. Sun, and X. Xu, Controlled synthesis of NiS nanoparticle/CdS nanowire heterostructures via solution route and their optical properties, *Mater. Sci. Eng. B*, 178(2013), No. 1, p. 109.

[5] Y.B. Li, H.F. Wang, H.M. Zhang, P.R. Liu, Y. Wang, W.Q. Fang, H.Q. Yang, Y. Li, and H.J. Zhao, A {0001} faceted single crystal NiS nanosheet electrocatalyst for dye-sensitised solar cells: sulfur-vacancy induced electrocatalytic activity, *Chem. Commun.*, 50(2014), p. 5569.

[6] C.J. Tang, C.H. Zang, J.F. Su, D.M. Zhang, G.H. Li, Y.S. Zhang, and K. Yu, Structure and magnetic properties of flower-like α-NiS nanostructures, *Appl. Surf. Sci.*, 257(2011), No. 8, p. 3388.

[7] H.C. Ruan, Y.F. Li, H.Y. Qiu, and M.D. Wei, Synthesis of porous NiS thin films on Ni foam substrate via an electrodeposition route and its application in lithium-ion batteries, *J. Alloys Compd.*, 588(2014), p. 357.

[8] Z.Q. Wang, X. Li, Y. Yang, Y.J. Cui, H.G. Pan, Z.Y. Wang, B.L. Chen, and G.D. Qian, Highly dispersed β-NiS nanoparticles in porous carbon matrices by a template metal–organic framework method for lithium-ion cathode, *J. Mater. Chem. A*, 2(2014), p. 7912.

[9] S.B. Ni, X.L. Yang, and T. Li, Fabrication of a porous NiS/Ni nanostructured electrode via a dry thermal sulfuration method and its application in a lithium ion battery, *J. Mater. Chem.*, 22(2012), p. 2395.

[10] Y. Wang, Q.S. Zhu, L. Tao, and X.W. Su, Controlled-synthesis of NiS hierarchical hollow microspheres with different building blocks and their application in lithium batteries, *J. Mater. Chem.*, 21(2011), p. 9248.

[11] K. Aso, A. Hayashi, and M. Tatsumisago, Preparation conditions of NiS active material in high-boiling solvents for all-solid-state lithium secondary batteries, *New J. Chem.*, 38(2014), p. 1731.

[12] H.M. Chuang, C.T. Li, M.H. Yeh, C.P. Lee, R. Vittal, and K.C. Ho, A coral-like film of Ni@NiS with core–shell particles for the counter electrode of an efficient dye-sensitized solar cell, *J. Mater. Chem. A*, 2(2014), p. 5816.

[13] H.C. Sun, D. Qin, S.Q. Huang, X.Z. Guo, D.M. Li, Y.H. Luo, and Q.B. Meng, Dye-sensitized solar cells with NiS counter electrodes electrodeposited by a potential reversal technique, *Energy Environ. Sci.*, 4(2011), p. 2630.

[14] J.L. Meng, Z.M. Yu, Y. Li, and Y.D. Li, PdS-modified CdS/NiS composite as an efficient photocatalyst for H_2 evolution in visible light, *Catal. Today*, 225(2014), p. 136.

[15] Z.H. Chen, P. Sun, B. Fan, Z.G. Zhang, and X.M. Fang, *In situ* template-free ion-exchange process to prepare visible-light-active g-C_3N_4/NiS hybrid photocatalysts with enhanced hydrogen evolution activity, *J. Phys. Chem. C*, 118(2014), No. 15, p. 7801.

[16] Q. Pan, J. Xie, S.Y. Liu, G.S. Cao, T.J. Zhu, and X.B. Zhao, Facile one-pot synthesis of ultrathin NiS nanosheets anchored on graphene and the improved electrochemical Li-storage properties, *RSC Adv.*, 3(2013), p. 3899.

[17] Q. Pan, J. Xie, T. Zhu, G. Cao, X. Zhao, and S. Zhang, Reduced graphene oxide-induced recrystallization of NiS nanorods to nanosheets and the improved Na-storage properties, *Inorg. Chem.*, 53(2014), No. 7, p. 3511.

[18] Y.H. Zhang, L. Guo, L. He, K. Liu, C.P. Chen, Q. Zhang, and Z.Y. Wu, Controlled synthesis of high-quality nickel sulfide chain-like tubes and echinus-like nanostructures by a solution chemical route, *Nanotechnology*, 18(2007), No. 48, p. 485609.

[19] X.C. Jiang, Y. Xie, J. Lu, L.Y. Zhu, W. He, and Y.T. Qian, A hydrogen bond-template route to nickel sulfide submicrotubes, *Adv. Mater.*, 13(2001), p. 1278.

[20] W.Q. Zhang, L.Q. Xu, K.B. Tang, F.Q. Li, and Y.T. Qian, Solvothermal synthesis of NiS 3D nanostructures, *Eur. J. Inorg. Chem.*, 2005(2005), No. 4, p. 653.

[21] L.W. Mi, Y.F. Chen, W.T. Wei, W.H. Chen, H.W. Hou, and Z. Zheng, Large-scale urchin-like micro/nano-structured NiS: controlled synthesis, cation exchange and lithium-ion battery applications, *RSC Adv.*, 3(2013), p. 17431.

[22] H.B. Li, L.L. Chai, X.Q. Wang, X.Y. Wu, G.C. Xi, Y.K. Liu, and Y.T. Qian, Hydrothermal growth and morphology modification of β-NiS three-dimensional flowerlike architectures, *Cryst. Growth Des.*, 7(2007), No. 9, p. 1918.

[23] H. Zhou, B.L. Lv, D. Wu, and Y.H. Sun, Hydrothermal synthesis and characterization of NiS flower-like architectures, *Particuology*, 10(2012), No. 6, p. 783.

[24] Z.C. Wu, C. Pan, T.W. Li, G.J. Yang, and Y. Xie, Formation of uniform flowerlike patterns of NiS by macrocycle polyamine assisted solution-phase route, *Cryst. Growth Des.*, 7(2007), No. 12, p. 2454.

[25] F.M. Zhan, B.Y. Geng, Y.J. Guo, and L. Wang, One-step synthesis of hierarchical carnation-like NiS superstructures via a surfactant-free aqueous solution route, *J. Alloys Compd.*, 482(2009), No. 1-2, p. L1.

[26] P.F. Yang, B. Song, R. Wu, Y.F. Zheng, Y.F. Sun, and J.K. Jian, Solvothermal growth of NiS single-crystalline nanorods, *J. Alloys Compd.*, 481(2009), No. 1-2, p. 450.

[27] A. Ghezelbash, M.B. Sigman, and B.A. Korgel, Solventless synthesis of nickel sulfide nanorods and triangular nanoprisms, *Nano Lett.*, 4(2004), No. 4, p. 537.

[28] J. Yang, X. Duan, Q. Qin, and W. Zheng, Solvothermal synthesis of hierarchical flower-like β-NiS with excellent electrochemical performance for supercapacitors, *J. Mater. Chem. A*, 1(2013), p. 7880.

[29] M. Salavati-Niasari, G. Banaiean-Monfared, H. Emadi, and M. Enhessari, Synthesis and characterization of nickel sulfide nanoparticles via cyclic microwave radiation, *C. R. Chim.*, 16(2013), No. 10, p. 929.

[30] K. Nithima, O. Areeporn, K. Jinda, and O. Makoto, Formation of MnS- and NiS-montmorillonites by solid-solid reactions, *Appl. Clay Sci.*, 43(2009), p. 238.

[31] J.H. Jiang, R. Yu, R. Yi, W.Q. Qin, G.Z. Qiu, and X.H. Liu, Biomolecule-assisted synthesis of flower-like NiS microcrystals via a hydrothermal process, *J. Alloys Compd.*, 493(2010), No. 1-2, p. 529.

[32] L.L. Wang, Y.C. Zhu, H.B. Li, Q.W. Li, and Y.T. Qian, Hydrothermal synthesis of NiS nanobelts and NiS_2 microspheres constructed of cuboids architectures, *J. Solid State Chem.*, 183(2010), No. 1, p. 223.

[33] P.T. Zhao, Q.M. Zeng, and K.X. Huang, Fabrication of β-NiS hollow sphere consisting of nanoflakes via a hydrothermal process, *Mater. Lett.*, 63(2009), No. 2, p. 313.

[34] Z.Y. Meng, Y.Y. Peng, W.C. Yu, and Y.T. Qian, Solvothermal synthesis and phase control of nickel sulfides with different morphologies, *Mater. Chem. Phys.*, 74(2002), No. 2, p. 230.

[35] S.H. Yu and M. Yoshimura, Fabrication of powders and thin films of various nickel sulfides by soft solution-processing routes, *Adv. Funct. Mater.*, 12(2002), No. 4, p. 277.

[36] X.P. Shen, J.Q. Sun, G.X. Wang, J.S. Park, and K.M. Chen, A facile single-source approach to urchin-like NiS nanostructures, *Mater. Res. Bull.*, 45(2010), No. 7, p. 766.

[37] Q.T. Pan, K. Huang, S.B. Ni, F. Yang, and D.Y. He, Synthesis of flower- and rod-like nickel sulfide nanostructures by an organic-free hydrothermal process, *Mater. Res. Bull.*, 43(2008), No. 6, p. 1440.

[38] J.H. Wang, Z. Cheng, J.L. Brédas, and M.L. Liu, Electronic and vibrational properties of nickel sulfides from first principles, *J. Chem. Phys*., 127(2007), p. 214705.

[39] D.W. Bishop, P.S. Thomas, and A.S. Ray, Micro Raman characterization of nickel sulfide inclusions in toughened glass, *Mater. Res. Bull.*, 35(2000), No. 7, p. 1123.

[40] H.T. Zhang, G. Wu, and X.H. Chen, Synthesis and magnetic properties of NiS_{1+x} nanocrystallines, *Mater. Lett.*, 59(2005), No. 28, p. 3728.

[41] J.T. Sparks and T. Komoto, Metal-to-Semiconductor Transition in Hexagonal NiS, *Rev. Mod. Phys.*, 40(1968), p. 752.

[42] C. Dewitt, B. Dreyfus, and P.D. de Gennes, *Low Temperature Physics*, Gordon and Beach, New York, 1962, p. 413.

[43] M. Salavati-Niasari, F. Davar, and M. Mazaheri, Synthesis, characterization and magnetic properties of NiS_{1+x} nanocrystals from [bis(salicylidene)nickel(II)] as new precursor, *Mater. Res. Bull.*, 44(2009), No. 12, p. 2246.

[44] F. Cao, R.X. Liu, L. Zhou, S.Y. Song, Y.Q. Lei, W.D. Shi, F.Y. Zhao, and H.J. Zhang, One-pot synthesis of flowerlike Ni_7S_6 and its application in selective hydrogenation of chloronitrobenzene, *J. Mater. Chem.*, 20(2010), p. 1078.

[45] R.H. Kodama, S.A. Makhlouf, and A.E. Berkowitz, Finite size effects in antiferromagnetic NiO nanoparticles, *Phys. Rev. Lett.*, 79(1997), p. 1393.

[46] A. Sobhani and M. Salavati-Niasari, Synthesis, characterization, optical and magnetic properties of a nickel sulfide series by three different methods, *Superlattices Microstruct.*, 59(2013), p. 1.